Fabrication of pyramidal probes with various periodic patterns and a single nanopore

Seong Soo Choi, Myoung Jin Park, Chul Hee Han, Sae Joong Oh, Sang Hun Han, Nam Kyou Park, Yong-Sang Kim, and Hyuck Choo

---

Articles you may be interested in

Electrical pulse fabrication of graphene nanopores in electrolyte solution
Appl. Phys. Lett. **106**, 203109 (2015); 10.1063/1.4921620

Mechanisms of material removal and mass transport in focused ion beam nanopore formation
J. Appl. Phys. **117**, 085304 (2015); 10.1063/1.4913449

Fabrication of faceted nanopores in magnesium
Appl. Phys. Lett. **103**, 243101 (2013); 10.1063/1.4841515

Direct fabrication of nanopores in a metal foil using focused ion beam with in situ measurements of the penetrating ion beam current
Rev. Sci. Instrum. **80**, 125102 (2009); 10.1063/1.3270958

Observation of isolated nanopores formed by patterned anodic oxidation of aluminum thin films
Appl. Phys. Lett. **88**, 233112 (2006); 10.1063/1.2212535

Fabrication of pyramidal probes with various periodic patterns and a single nanopore

Seong Soo Choi,[a] Myoung Jin Park, Chul Hee Han, and Sae Joong Oh
Research Center for Nanobio Science, Sun Moon University, Ahsan, Chungnam 31460, South Korea

Sang Hun Han and Nam Kyou Park
School of Electrical Engineering, Seoul National University, Seoul 08826, South Korea

Yong-Sang Kim
School of Electronic and Electrical Engineering, Sungkyunkwan University, Suwon, Gyeonggi-Do 16419, South Korea

Hyuck Choo
School of Electrical Engineering, California Institute of Technology, Pasadena, California 91125

The nanometer-scale patterned pyramidal probe with an electron beam-induced nanopore on the pyramid apex is an excellent candidate for an optical biosensor. The nanoapertures surrounded with various periodic groove patterns on the pyramid sides were fabricated using a focused ion beam technique, where the optical characteristics of the fabricated apertures with rectangular, circular, and elliptical groove patterns were investigated. The elliptical groove patterns on the pyramid were designed to maintain an identical distance between the grooves and the apex for the surface waves and, among the three patterns, the authors observed the highest optical transmission from the elliptically patterned pyramidal probe. A 10^3-fold increase of the transmitted optical intensity was observed after patterning with elliptical grooves, even without an aperture on the pyramid apex. The nanopore on the apex of the pyramid was fabricated using electron beam irradiation and was optically characterized. © 2015 American Vacuum Society. [http://dx.doi.org/10.1116/1.4935560]

I. INTRODUCTION

There has been tremendous interest in plasmonic nanoapertures on pyramidal probes for single-molecule biosensor applications where, specifically, to obtain plasmonic optical effects through a tiny nanometer-sized hole on the pyramid, it would be desirable to fabricate a periodic nanopatterning on the pyramid. The enhancement of light transmission through a nanometer-sized aperture surrounded by periodic patterns on the input side of a flat plane has been previously reported,[1,2] but an equivalent setup would be difficult to fabricate on a hollow pyramid because of the difficulty in fabricating the groove patterns on its inner side. A directional beaming effect through an aperture with a periodic pattern on the exit side of a flat membrane has been reported,[3] and slit groove patterning fabricated on the exit side of the input beam has also been reported, which provided controllable far-field focusing.[4,5] Plasmonic optical effects can be obtained by patterning periodic grooves on the outside of the pyramid, and we have previously reported the effect of periodically patterned grooves upon the enhancement of the transmitted beam through an aperture on the pyramid.[6–8] The nanofocusing that exists at the aperture on a conical probe[9] and at the nanograting on a pyramidal tip[10] have been reported as a "plasmonic lens effect," where a conical plasmonic probe with a 100 nm-diameter aperture surrounded by a circular grating was found to provide better focusing with increased intensity at the apex area compared to that of a pyramidal probe without groove patterns. Also, a ~100 nm-diameter focal spot with a tenfold

increase in optical intensity at the apex of a conical probe has been obtained using a circular grating pattern to excite surface plasmon polaritons.[9] Enhancement of the optical intensity through a pyramidal aperture has been reported for groove patterns whose pitch matched the surface plasmon wavelength,[10] while three-dimensional nanofocusing at the apex of a pyramidal probe patterned with square grooves[11] and a nanofocusing plasmon waveguide on a two-dimensional plane[12] have also been reported. A pyramidal cavity array has been exploited as an efficient substrate for surface-enhanced Raman spectroscopy,[13] whereas a nanohole array on a flat Au membrane has also been used as a flow-through plasmonic sensing device.[14] The pyramidal nanoaperture has been found to provide excellent light confinement inside a V-shaped cavity,[14,15] and an enhanced optical throughput via cavity resonance[16,17] has also been reported. In addition, the pyramidal nanoaperture also provides an enhanced nanofocusing on top of the aperture.[10,12]

Recently, deoxyribonucleic acid translocation experiments using a solid state SiN nanopore have been reported,[18] in addition to the fabrication of a nanopore on an Au-coated pyramid.[19] An electron beam-induced nanopore inside a pyramidal Au aperture can be used as an optical nanobiosensor, while placing the nanopore on the apex of a thick pyramidal membrane would be ideal because of its mechanical stability during processing and the enhanced optical output that can be provided with a proper groove-patterning on the pyramid. In this paper, we report the fabrication of pyramidal nanoapertures with various types of groove patterns for better optical focusing and optical enhancements, and of an electron

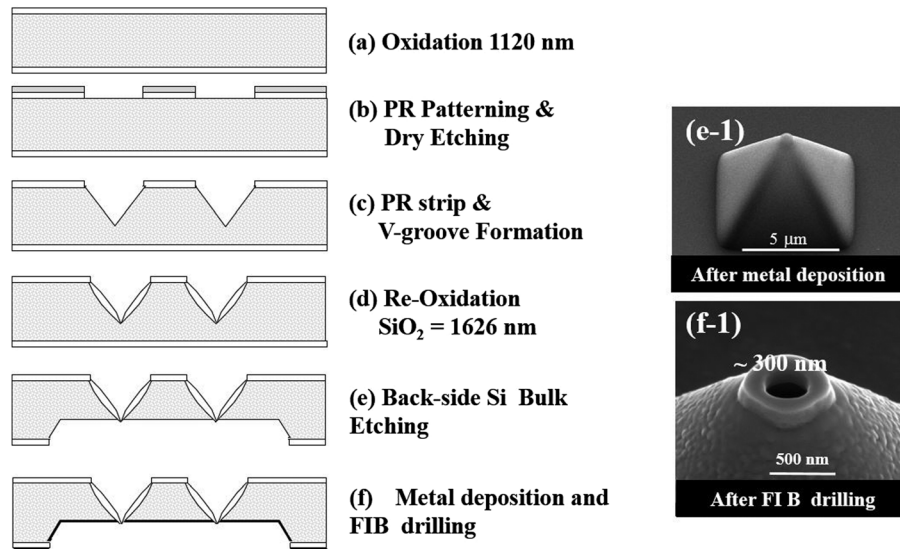[a]Electronic mail: sscphy2010@gmail.com

FIG. 1. Schematic of the pyramidal probe array fabrication using a conventional Si microfabrication process. Photolithographic patterns transfer (c), followed by low temperature thermal oxidation at 1000 °C in (d), backside bulk Si TMAH etching in (e), metal deposition and FIB beam drilling (f) are shown. FESEM images of the (e-1) fabricated pyramid with a nanoflower-type cavity at the apex and (f-1) the aperture drilled into the pyramid apex using FIB.

beam-induced nanopore inside an Au cavity on top of the pyramid.

II. EXPERIMENTAL PROCESS

A. Fabrication of pyramidal probe

The nanoprobes on top of the pyramidal array with micron-sized square patterns were fabricated using the conventional Si microfabrication process, including photolithography, wet etching, stress-induced thermal oxidation, and metal sputter deposition, as shown in Fig. 1. The pitch of the pyramidal patterns ranged from 10 to 30 μm depending upon the pattern size, while the pattern size also was varied from 5 to 30 μm for different experimental purposes. The stress-induced thermal oxidation performed at low temperatures less than 1000 °C provided the thinner oxide at the apex of the pyramid shown in Fig. 1(d) and, after backside Si etching for more than 10 h using a tetramethylamonium hydroxide (TMAH) solution, an oxide aperture could be formed at the apex. Subsequently, an Al thin film 200 nm thick was sputter deposited using a two-step deposition technique, which produced a nanoflower-type cavity on the apex of the pyramid, as shown in Fig. 1(e-1), where the height of the nanoflower

cavity was measured to be ∼200 nm [Fig. 1(f-1)]. The pyramidal apex was then drilled to produce a circular cavity opening using a 30 keV Ga focused ion beam technique (FIB; Helios Dual Beam, FEI), whose detailed fabrication process is given elsewhere.[20,21] Figure 2 presents typical field emission scanning electron microscope (FESEM, Hitachi 4800) images of the fabricated pyramidal array including a top view (a) and a tilted view (b).

B. Finite-difference time-domain simulation for pyramidal probe

We carried out two-dimensional finite-difference time-domain (FDTD) simulations for the pyramidal probes with and without groove patterns. The material properties of the models (Al and SiO_2) were taken into consideration with a complex permittivity ε given by the Drude–Lorentz dispersion model and the relative permeability $\mu = 1$. For Al and SiO_2, the values of $\varepsilon(Al) = -20.60 + 0.436i$ and $\varepsilon(SiO_2) = 2.133$ were used. Using these parameters on the cross-section of the structures, the time-harmonic Maxwell equations were solved to obtain the optical intensity profile spanning these pyramidal structures. The pyramidal probe with a 100 nm diameter consisted of a 200 nm-thick Al film on a 100 nm-thick SiO_2
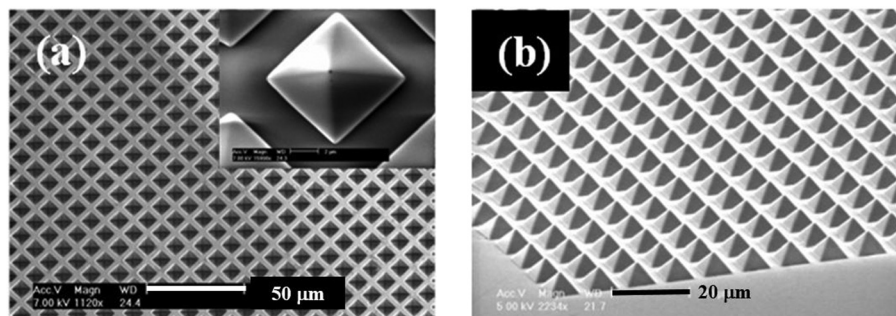

FIG. 2. FESEM images of the microfabricated pyramidal array sample showing the (a) top view and (b) tilted view.
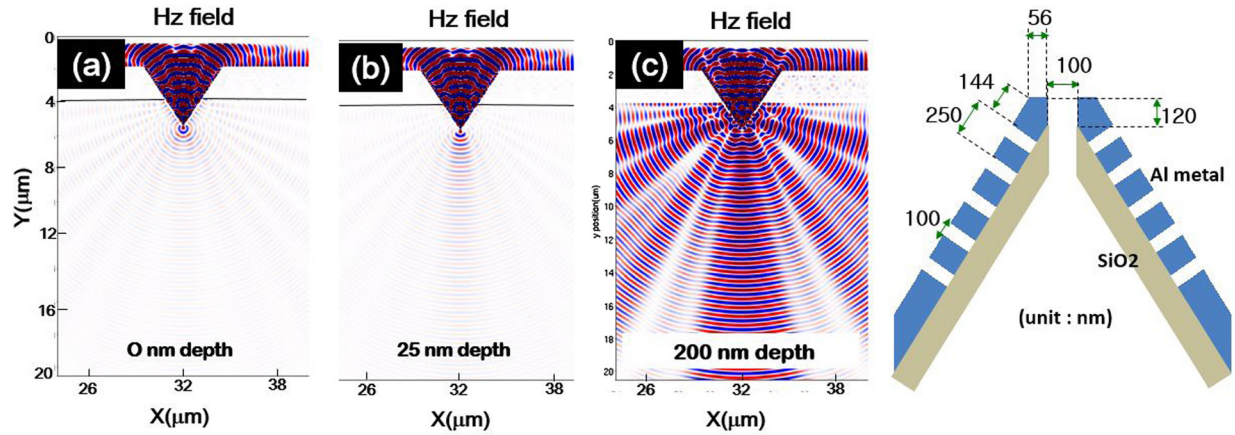
FIG. 3. (Color online) FDTD simulation of the Hz field for the transmitted optical field through a pyramidal probe with and without a grating pattern. The depth of the patterns is varied from (a) 0, (b) 25, and (c) 200 nm. The aperture diameter, the pattern width, and the groove pitch are set as 100, 100, and 250 nm, respectively, as shown in (d). The Hz field intensities through a pyramidal probe with a 200 nm deep grating are the strongest.

pyramid, and the pitch and the width of the grooves were set to be 250 and 100 nm, respectively. The two dimensional simulations for the transverse magnetic field mode (E_x, E_y, and H_z) with the arbitrary field intensity level were conducted. Figure 3 presents the magnetic H_z field intensity distributions for pyramidal apertures with and without groove patterns where, without groove patterns, an isotropic transmitted optical beam can be seen [Fig. 3(a)]. However, for groove patterns with a depth of 25 nm, a slightly increased magnetic field (H_z) intensity into the propagation direction is seen [Fig. 3(b)] and, further, for groove patterns with a depth of 200 nm, a strong H_z field intensity into the propagating direction with a directional beaming is clearly seen [Fig. 3(c)]. The ratios of the transmitted output intensities to the input intensities for groove depths of 0, 25, 100, and 200 nm are calculated to be 0.068, 0.104, 0.348, and 2.79, respectively (supplementary material 1).[22] These results present an exponential dependency of the transmitted optical intensities upon the groove thickness. However, owing to the limits of the two-dimensional FDTD simulation, a qualitative comparison with the experimental results from a three-dimensional pyramidal probe requires a more detailed simulation.

C. Fabrication of patterned probe and its optical characterization

Fabrication of the three types of groove patterns was carried out using a 30 keV Ga ion FIB technique producing the rectangular patterns [Fig. 4(a)], circular patterns [Fig. 4(b)], and elliptical groove patterns [Fig. 4(c)], as shown in Fig. 4. The elliptical groove pattern is designed to provide an equal sidewall distance from the apex of the pyramid to each groove, where the equidistant grooves on the sidewalls can provide a combination of four quadrant ellipses, as viewed from the top in Fig. 4(c). The rectangular groove patterns provided the least amount of symmetry in terms of equidistant points from the top of the pyramid. All groove patterns were designed with 100 nm depth and 100 nm width, while the diameters of the apertures were varied and the drilled groove pitches ranged from 500 to 250 nm along the sidewall. Figure 5 presents FESEM images of the pyramidal probes with circular groove patterns (top view) and with elliptical groove patterns (bottom view). The pitches of the grooves ranging from 250 to 500 nm, stepped by 50 nm between each pitch value, were drilled on the pyramidal sidewalls for both patterns, while the diameters for the circular groove patterns
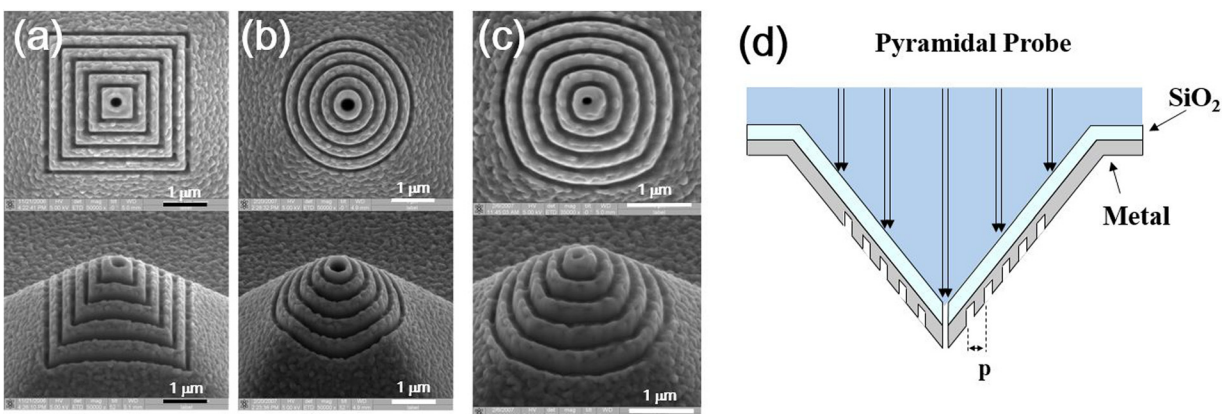

FIG. 4. (Color online) (a) Rectangular, (b) circular, and (d) elliptic periodic groove patterns fabricated using 30 keV FIB are shown in top view (upper) and tilted view (lower). (d) Schematic of the pyramidal probe (side view).

JVST B - Nanotechnology and Microelectronics: Materials, Processing, Measurement, and Phenomena
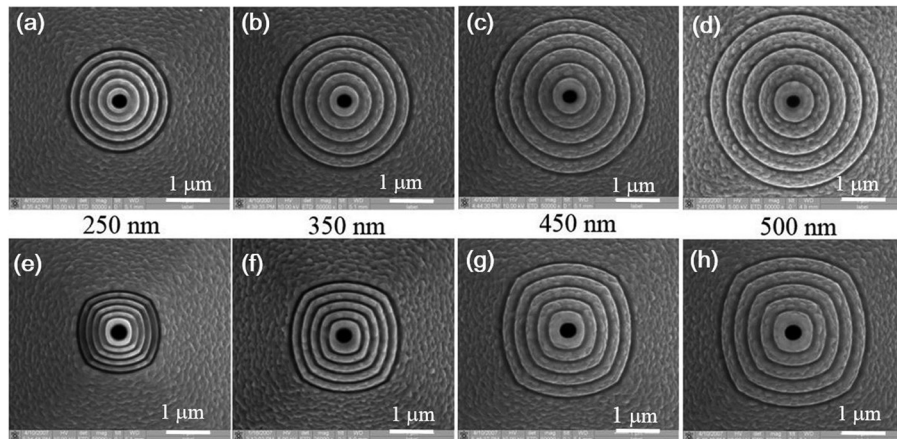
FIG. 5. FESEM images of the nanoapertures with circular groove patterns (upper) and elliptical patterns (lower), where the pitches along the side wall are drilled at [(a) and (e)] 250, [(b) and (f)] 350, [(c) and (g)] 450, and [(d) and (h)] 500 nm for both patterns with a pitch step of 50 nm.

and elliptic apertures were 370 and 430 nm, respectively, with less than 5% deviation.

Measurements of the light transmission through the nanoapertures were carried out in a scanning near-field optical microscope (WiTec AlphaSNOM), where the transmitted far field intensity was measured using a 532 nm wavelength neodymium-doped yttrium aluminum garnet laser system and an optical microscope (ECLIPSE Ti-U, Nikon) equipped with a spectrophotometer (Acton SpectraPro 2300i, Princeton Instruments). The ~2 mW laser beam was illuminated onto the inner side of a metal-coated SiO_2 pyramidal structure, as illustrated by the black arrows in Fig. 4(d), and the transmittance was measured as the ratio of the output intensity normalized to the aperture area to the input intensity normalized to a Gaussian beam area with a 3 μm diameter.

The dependence of the transmittance upon the groove pitch is presented in Fig. 6, where apertures with elliptically patterned grooves with pitch values less than 350 nm exhibit a drastic increase in the transmittance, reaching a maximum of 0.06 at 250 nm in Fig. 6(a), which corresponds to a maximum output power of 3.4 μW. Considering the wavelength of a surface plasmon at an Al/air interface ($\lambda_{spp} = 519$ nm),

the surface wave travels along the sidewall and then interacts with the groove structures to provide a constructive interference for a pitch value of ~260 nm. For pitches less than 260 nm, the reduced transmitted output intensity is likely owing to a decreased coupling of the surface wave with the groove structures. In Fig. 6(b), the transmittance values are constant for $0.6 < (d/\lambda) < 1.2$, where d is the aperture diameter and λ is the input wavelength, though the transmittance increases with decreasing values of (d/λ) below 0.6. A maximum optical power of 45 μW was measured, whose corresponding transmittance is 4.8 for $(d/\lambda) = 0.3$. The phenomenon of increased transmittance with smaller (d/λ) values can be attributed to fact that backward scattering through the aperture increases with decreasing aperture diameter.[23,24] When the aperture diameter is much larger than the input wavelength (λ), the transmitted intensity will be a sharp Gaussian distribution profile. However, for a (d/λ) value ~0.6, the transmitted intensity distribution becomes a broader Gaussian distribution profile with an increased backward scattered intensity comprising 6.6% of the maximum intensity at the central axis of the Gaussian intensity profile. For $0.1 < (d/\lambda) < 0.3$, the transmitted Gaussian intensity
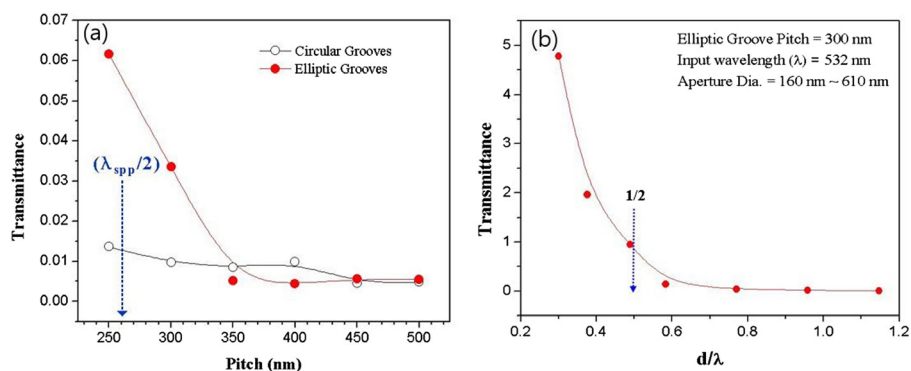

FIG. 6. (Color online) (a) Transmittance vs groove pitch using an input laser wavelength of 532 nm. The transmittances for apertures with elliptical groove patterns (closed red circles) become greater than those with circular groove patterns (open black circle) for groove pitches less than 350 nm. An arrow marks the pitch value of the greatest transmittance $\lambda_{spp}/2 = \sim 260$ nm, where $\lambda_{spp} = 519$ nm is the wavelength of a surface plasmon at an Al/air interface. (b) Transmittance for the pyramidal aperture with an elliptical groove pitch of 300 nm vs d/λ, where d is the aperture diameter and λ is the input wavelength. The arrow marks $0.5(d/\lambda)$, lower than which the transmittance, shows an increase. Transmittance values are the ratio of the input optical power normalized to its Gaussian beam area to the transmitted optical power normalized to the aperture area.
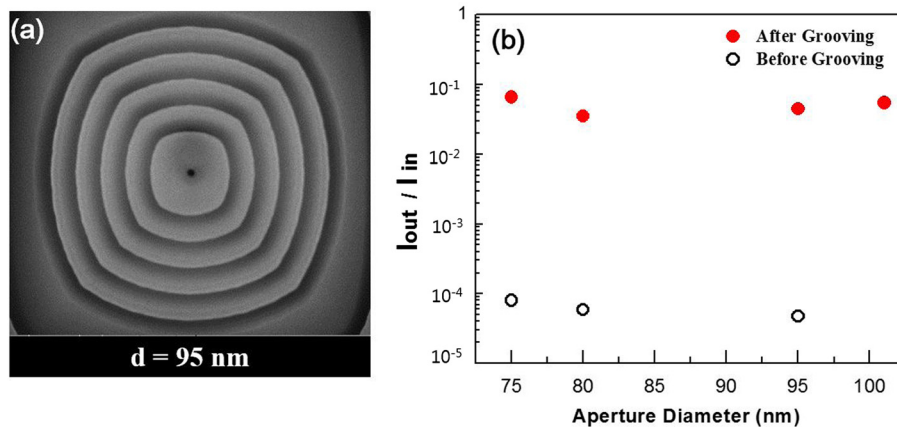
FIG. 7. (Color online) (a) SEM image of an aperture 95 nm in diameter surrounded with elliptically patterned grooves whose depth, width, and pitch are 100, 100 and 250 nm, respectively. (b) Transmittances through the nanoaperture without (open circles) and with (solid circles) the fabricated elliptical groove patterns. Enhanced transmittance with a 10^3-fold increase is seen with the presence of the elliptical groove pattern.

profile is much broader with this decreasing value of (d/λ). For a (d/λ) value ~0.1, the backward scattered intensity increases to comprise up to 38% of the maximum output intensity, so the transmittance will increase owing to an increased coupling of the backward scattered surface wave with the groove structures. However, for $(d/\lambda) \ll 0.1$, or as (d/λ) goes to zero, the aperture will be closed and the transmitted intensity should be zero. Hence, our data agree well with the other reports.[23]

In addition, we found that the optical enhancement rates for the elliptical groove-patterned pyramidal probes are greater than those for the rectangular groove patterns by a factor of 2.61 (supplementary material 2).[22]

We designed another set of nanoapertures on pyramids with a 200 nm thick Al coating using three slightly different aperture diameters of 75, 80, and 95 nm. Figure 7(a) shows an FESEM image of a 95 nm-diameter aperture surrounded by five elliptical groove patterns 100 nm wide, 100 nm deep, and a 250 nm pitch. The ratios of output power to input power as a function of aperture diameters are presented in Fig. 7(b), where a 1000-fold increase in the transmitted optical power is observed between apertures without and with elliptical grooves patterned on the pyramid. Without patterning, the transmitted output optical powers for the pyramidal probes with 75, 80, and 95 nm aperture diameters for a 1.4 mW input power are 0.11, 0.08, and 0.07 μW, respectively; while with patterning, the transmitted output optical powers for the

pyramidal probes with 75, 80, and 95 nm aperture diameters are 89.8, 46.2, and 57.7 μW, respectively. The noise level of optical intensities through a pyramidal probe without an aperture and patterns for a 532 nm wavelength input laser is measured to be ~50 nW or less. A slight increase in the transmitted optical power with decreasing aperture diameter is also observed with and without patterning.

Optical characterizations for input wavelengths of 532 and 780 nm were also performed several months after the initial optical measurements, where the output optical intensities for a 780 nm input wavelength are higher than those for a 532 nm input wavelength. These experimental results can be attributed to a greater overlap of the photonic modes into the localized surface plasmon modes in the groove for an input wavelength of 780 nm than for 532 nm.[25] Higher transmittances at 532 nm than those found in the previous initial measurements are also observed owing to the reduced diameter of the apertures by ~10 nm because of Au migration under the room temperature storage environment (supplementary material 3).[22]

To examine in detail the influence of the grooves upon the optical transmission, three different types of pyramidal probes on SiO$_2$ pyramidal probes coated with a 200 nm-thick Al layer were fabricated without apertures: those possessing no grooves and those possessing 10 or 25 nm-deep grooves on the exit side of the pyramid (Fig. 8). The width and the pitch for all three samples were 100 and 250 nm, respectively, and,
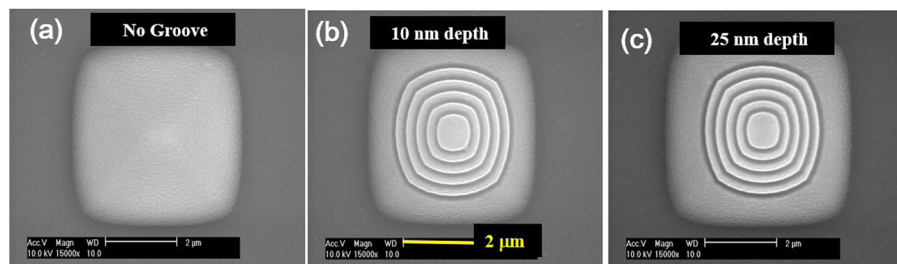
FIG. 8. (Color online) FESEM images of pyramidal probes with (a) no patterning, and those possessing elliptical groove patterns with a depth of (b) 10 and (c) 25 nm. The width and the pitch of the grooves are designed to be 100 and 250 nm, respectively. The ratio of the output optical power to the input optical power presents a 1000-fold increase after groove patterning is introduced.

JVST B - Nanotechnology and Microelectronics: Materials, Processing, Measurement, and Phenomena

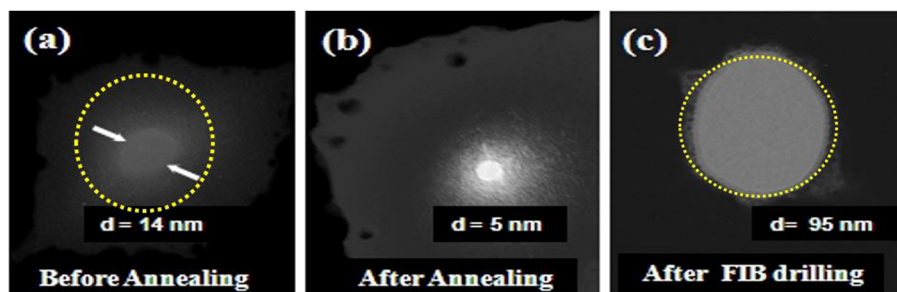FIG. 9. (Color online) TEM images of the FESEM-induced nanopore with (a) a 14 nm diameter before TEM annealing, (b) a 5 nm diameter after TEM annealing, and (c) a 95 nm diameter aperture after FIB drilling.

to calibrate the depth of the drilled groove, elliptical grooves were drilled on a flat Au film and the drilled depths of the grooves were measured by atomic force microscopy (XE-100, PSIA, Inc.) (supplementary material 3).[22] The transmitted optical powers for the pyramidal probes with 0, 10, and 25 nm groove depths are measured to be 12 nW, 20.1, and 45 μW, respectively, as tabulated in Table I, while the corresponding ratios of the output to input power for the patterned probes with 10 and 25 nm groove depths are 1.3×10^{-2} and 3.3×10^{-2}, respectively. Hence, a $\sim 10^{3}$-fold increase in the transmitted optical power for the patterned probes is observed over that of probes without patterning, which can be attributed to the resonant transmission from the input optical wave photon mode overlapping the localized surface plasmon states in the groove cavities.[25,26] We also examined the optical characteristics of the pyramidal probes containing apertures and those with grooves but no apertures using the optical microscope with a spectrophotometer. The pyramidal apertures with diameters of 129, 124, and 116 nm were drilled without groove patterns, and the optical intensities from those apertures are found to be ~ 12 nW. However, for pyramids with periodic elliptical groove patterns optical spots are clearly visible and, in addition, two resonant peaks in the transmitted optical intensity distribution are observed (supplementary material 3).[22]

D. Fabrication of an Au nanopore inside an Au cavity

We fabricated a nanopore inside an Au nanoflower-type cavity on the top of the pyramid using 2 keV electron beam irradiation for 5 min, where the transmission electron microscope (TEM, JEM 2010 and JEM 3011 HR) images of the 14 nm-diameter nanopore on the diffuse membrane inside the Au cavity can be seen in Fig. 9(a). After 5 min of annealing using a 200 keV TEM electron beam, the pore diameter was reduced to 5 nm [Fig. 9(b)], and a FIB drilling technique

was subsequently employed to remove the diffuse membrane [Fig. 9(c)]. Optical characterizations were carried out after each process, and the optical intensities after each annealing process as well as the optical intensity through an Au aperture with a 100 nm diameter on a 200 nm-thick Au film are presented in Table II. The ratios of the output optical intensity to the input optical intensity are measured to be 2.2×10^{-2} and are almost constant for all three experimental conditions. Under electron beam exposure, the diffused carbon-contained membrane did not present any influence upon the optical intensity, possibly because the membrane thickness of 10 nm or less was well below the Au skin depth (~ 20 nm). There is found a 46-fold optical enhancement for the apertures on the pyramid over the optical intensity through a 100 nm-diameter Au aperture on flat Au film. This optical enhancement can be attributed to the coupling of local surface plasmons in the Au cavity with the input photon beam in the pyramidal V groove.[17]

III. CONCLUSION

We have fabricated nanopatterned pyramidal probes with a nanopore inside an Au cavity on the pyramidal apex:

(1) We have examined the coupling of a backward-diffracted surface wave with the patterned grooves on the exit side of the pyramid. With decreasing aperture diameters, increased optical powers were observed for $(d/\lambda) < 0.5$, with a maximum output intensity obtained for $(d/\lambda) = \sim 0.3$, owing to increased backward surface waves from the pyramidal aperture. However, a higher output intensity could be achieved for $(d/\lambda) = \sim 0.1$. These enhancements could be attributed to coupling of the backward-scattered surface waves with the periodic groove structures. In addition, constructive interference of the backscattered surface waves with the periodic groove structure presented an increased transmittance of 0.06 for a pitch of 260 nm.

(2) Coupling effects dependent upon the type of groove patterns on the exit sides of the pyramidal probes are investigated. The highest optical transmitted power are obtained from the elliptically patterned probes, which can be attributed to the fact that the backward-scattered surface wave interacts coherently with localized surface plasmons in the equidistant elliptical groove patterns on

TABLE I. Comparison data of the transmitted optical power for pyramidal probes without and with elliptical groove patterning.

Groove depth (nm)	P_{in} (mW)	P_{out} (μW)	P_{out}/P_{in}
0	1.1	0.012	1.5×10^{-5}
10	1.6	20.1	1.3×10^{-2}
25	1.4	~ 45	3.3×10^{-2}

TABLE II. Optical intensity data for the various apertures produced by the given experimental conditions. The ratios of the optical output intensities to the input intensities for various Au apertures (in bold face) are presented for comparison.

	λ_0	D (nm)	I_{in} ($\mu W/cm^2$)	I_{out} ($\mu W/cm^2$)	I_{out}/I_{in}	
After FIB drilling	532 nm	∼95	1662	37.5	**2.26×10^{-2}**	(c)
After E-Beam annealing		∼5	1430	32.7	**2.20×10^{-2}**	(b)
Before annealing at 10 keV		∼14	1684	39.0	**2.33×10^{-2}**	(a)
Au aperture on 200 nm thick plane		100	1380	2.3	**1.6×10^{-3}**	SO8 BDP II # 1-50-2

the sidewalls of pyramid, resulting in the highest transmitted optical power.

(3) Even without a nanoaperture on top of the pyramid, a 10^3-fold increase in transmitted optical power from an elliptically patterned pyramid is presented. These experimental observations indicate the strong coupling of the surface plasmonic modes with the photonic modes of the input beams.

(4) A nanopore is fabricated inside an Au cavity on top of the pyramid via electron beam irradiation and FIB and is optically characterized at three stages of fabrication. The ratios of the output intensity to the input intensity are almost constant (2.3×10^{-2}) for the three different experimental conditions, and the 46-fold optical enhancement over that found transmitted through a 100 nm-diameter Au nanoaperture on a 200 nm-thick flat plane can be attributed to coupling of the local surface plasmon in the Au cavity with the input photonic beam.

A nanopore on the apex of a pyramidal probe integrated with periodic groove patterns can be an excellent candidate for a single-molecule biosensor.

ACKNOWLEDGMENTS

[1]T. W. Ebbesen, H. J. Lezec, H. F. Ghaemi, T. Thio, and P. A. Wolff, Nature **391**, 667 (1998).

[2]T. Thio, K. M. Pellerin, R. A. Linke, H. J. Lezec, and T. W. Ebbesen, Opt. Lett. **26**, 1972 (2001).

[3]H. J. Lezec, A. Degiron, E. Devaux, R. A. Linke, L. Martin-Moreno, F. J. Garcia-Vidal, and T. W. Ebbesen, Science **297**, 820 (2002).

[4]F. Hao, R. Wang, and J. Wang, Opt. Express **18**, 15741 (2010).

[5]S. Kim, Y. Lim, H. Kim, J. Park, and B. Lee, Appl. Phys. Lett. **92**, 013103 (2008).

[6]S. S. Choi, D. W. Kim, Y. C. Kim, and M. J. Park, "The effect of groove shape on light transmission," *3rd International Conference on Surface Plasmon Photonics*, Dijon, France, 17–22 June (2007).

[7]D. W. Kim, Y. C. Kim, O. Suwal, V. Jha, M. J. Park, and S. S. Choi, Mater. Sci. Eng. B **149**, 242 (2008).

[8]S. S. Choi, O. K. Suwal, V. K. Jha, D. W. Kim, and M. J. Park, Curr. Appl. Phys. **9**, S131 (2009).

[9]Y. Wang, W. Srituravanich, C. Sun, and X. Zhang, Nano Lett. **8**, 3041 (2008).

[10]Y. Wang, Y. Y. Huang, and X. Zhang, Opt. Express **18**, 14004 (2010).

[11]N. C. Lindquist, P. Nagpal, A. Lesuffleur, D. J. Norris, and S. H. Oh, Nano Lett. **10**, 1369 (2010).

[12]H. Choo, M. K. Kim, M. Staffaroni, T. J. Seok, J. Bokor, S. Cabrini, P. J. Schuck, M. C. Wu, and E. Yablonovitch, Nat. Photonics **6**, 838 (2012).

[13]N. M. B. Perney, F. J. G. D. Abajo, J. J. Baumberg, A. Tang, M. C. Netti, M. D. B. Charlton, and M. E. Zoorob, Phys. Rev. B **76**, 035426 (2007).

[14]F. Eftekharl, C. Escobedo, J. Ferreira, X. Duan, E. M. Girotto, A. G. Broto, R. Gordon, and D. Sinton, Anal. Chem. **81**, 4308 (2009).

[15]M. Trupke *et al.*, Appl. Phys. Lett. **88**, 071116 (2006).

[16]C. Chen, N. Verellen, K. Lodewijks, L. Lagae, G. Maes, G. Borghs, and P. V. Dorpe J. Appl. Phys. **108**, 034319 (2010).

[17]M. Consonni, J. Hazart, G. Lérondel, and A. Vial, J. Appl. Phys. **105**, 084308 (2009).

[18]U. F. Keyser, B. N. Koeleman, S. V. Dorp, D. Krapf, R. M. Smeets, S. G. Lemay, N. H. Dekker, and C. Dekker, Nat. Phys. **2**, 473 (2006).

[19]S. S. Choi, M. J. Park, T. Yamaguchi, S. I. Kim, K. J. Park, and N. K. Park, Appl. Surf. Sci. **310**, 196 (2014).

[20]S. S. Choi, J. T. Ok, D. W. Kim, M. Y. Jung, and M. J. Park, J. Korean Phys. Soc. **45**, 1659 (2004).

[21]D. W. Kim, M. J. Park, C. H. Han, and S. S. Choi, Nanotechnology **16**, S304 (2005).

[22]See supplementary material at http://dx.doi.org/10.1116/1.4935560 for FDTD simulation for the optical output intensities (Supplementary Materials 1), ratios of the output intensities to the input intensities for the rectangular groove patterned aperture and for the elliptically patterned apertures (Supplementary Materials 2), and optical data from Nikon Optical microscope with a Princeston spectrophotometer and AFM data for drilled groove depths (Supplementary Materials 3).

[23]C. Obermüller and K. Karraia, Appl. Phys. Lett. **67**, 3408 (1995).

[24]A. Drezet, J. C. Woehl, and S. Huant, Phys. Rev. E **65**, 046611 (2002).

[25]S. A. Darmanyan and A. V. Zayats, Phys. Rev. B **67**, 035424 (2003).

[26]W.-C. Tan, T. W. Preist, J. R. Sambles, and N. P. Wanstall, Phys. Rev. B **59**, 12661 (1999).